scientific reports

Check for updates

OPEN

Complete preclinical evaluation of the novel antibody mimetic Nanofitin-IRDye800CW for diverse non-invasive diagnostic applications in the management of HER-2 positive tumors

Margherita Iaboni[1,5]✉, Federico Crivellin[1,5], Francesca Arena[1,5], Francesca La Cava[1], Alessia Cordaro[1], Francesco Stummo[1], Daniele Faletto[1], Simon Huet[2], Leo Candela[2], Jessy Pedrault[2], Eugenia R. Zanella[3], Andrea Bertotti[3,4], Francesco Blasi[1], Alessandro Maiocchi[1], Luisa Poggi[1] & Erika Reitano[1]

There are well-known limitations associated to the use of antibodies in the non-invasive detection of HER-2 expression. In fact, current procedures recommended for diagnostic purposes of HER-2 status are still invasive techniques. Here, a novel, smaller diagnostic probe, the anti-HER-2 Nanofitin conjugated to the fluorophore IRDye800CW (NF-800), underwent an in vitro/in vivo proof of concept study by Optical Imaging. NF-800 showed high affinity and specificity for the cellular target, and the ability to internalize into HER-2 positive cells. By ex vivo analysis, NF-800 showed a selective tumor accumulation in xenograft tumor models, and also a good tumor targeting efficacy in translational preclinical setups, such as orthotopic and patient-derived xenograft (PDX) models. In the latter, NF-800 was compared to the anti-HER-2 antibody Trastuzumab, displaying a large diagnostic advantage. Interestingly, NF-800 did not seem to share the same binding site with Trastuzumab and Pertuzumab, opening specific theragnostic opportunities for NF-800 in combination with standard-of-care antibodies.

Keywords Nanofitin, HER-2, Near-infrared, Optical imaging

Abbreviations

NF	Nanofitin
NF-800	Nanofitin-IRDye800CW
OI	Optical Imaging
PDX	Patient-derived xenograft
TBR	Tumor-to-background ratio
Tz	Trastuzumab

HER-2, a member of the ErbBs family of tyrosine kinase receptors, is a well-investigated transmembrane receptor overexpressed in many types of human cancers[1]. Amplification or overexpression of the HER-2 gene occurs in approximately 15–30% of breast cancers[1], but its alteration takes place also in other forms of cancer[2]. HER-2 exists as monomers on the cell surface and, not having a known direct activating ligand, is activated upon homo- and heterodimerization with another family member. This dimerization activates multiple downstream

[1]Bracco Research Centre, Bracco Imaging Spa, Via Ribes 5, 10010 Colleretto Giacosa, Turin, Italy. [2]Affilogic SAS, 24 Rue de La Rainière, 44300 Nantes, France. [3]Candiolo Cancer Institute – FPO IRCCS, Strada Provinciale 142, 10060 Candiolo, Turin, Italy. [4]Department of Oncology, University of Turin, Candiolo, Turin, Italy. [5]These authors contributed equally: Margherita Iaboni, Federico Crivellin and Francesca Arena. ✉email: margherita.iaboni@bracco.com

signalling pathways associated to proliferation, survival, differentiation, angiogenesis and invasion[3]. Therefore, it is considered an adverse prognostic factor associated with aggressive disease and worse clinical outcome.

From a prognostic and diagnostic perspective, the HER-2 status, defined as showing HER-2 gene amplification or protein overexpression, is predictive for response to targeted-therapies, which are mainly represented by the treatment with the humanized variants of monoclonal antibodies, *e.g.,*Trastuzumab and Pertuzumab[4,5]. To date, immunohistochemistry (IHC) and fluorescence in situ hybridization (FISH) are regarded as standard methods for determination of HER-2 status according to the ASCO/CAP guidelines[6,7]. However, apart from being an invasive technique, IHC cannot accurately reflect the HER-2 status both in real time and as a whole, due to the temporal and spatial heterogeneity of HER-2 expression in breast tumors, which may cause misguided treatment decisions[8–11].

In alternative, non-invasive imaging of cell receptors is a powerful technique that enables early identification of lesions as well as repetitive measurements and a more complete coverage[12]. Radiologists play an important role in diagnosis as well as in evaluating treatment response to guide surgical management or use of additional adjuvant therapies. However, there are no standards currently available for reporting molecular imaging assessment of breast tumor diagnosis and response to therapy.

Several studies have been reported on the development of tools for non-invasive detection of HER-2 expression, mostly dedicated to nuclear imaging and based on the use of appropriate radioderivatives of the anti-HER-2 monoclonal antibody Herceptin (*i.e.*, Trastuzumab)[13,14]. Despite the promising results obtained, these radioderivatives have limitations: the characteristic long biodistribution time and slow clearance of antibodies from the bloodstream, their accumulation into the liver, the requirement of the use of long-lived radioisotopes and imaging at late time points, exposing patients to a high radiation burden. For optimized diagnostic applications[15–17] specific smaller probes, with a faster biodistribution, are needed.

Among them, Nanofitins, developed by Affilogic, are artificial proteins derived from the hyperstable DNA binding protein Sac7d (7 kDa, 66 aminoacids), found in *Sulfolobus acidocaldarius*, from which they retain the original stability features of being thermophilic and acidophilic[18].

Nanofitins are selected by ribosome display libraries resulted by the full randomization of 10–14 amino acid residues in the DNA-binding site of Sac7d that allows enrichment for specific binders with high affinity for the target. Until now, several Nanofitins have been engineered over a wide range of targets and for different applications (*e.g.*, cell surface proteins[18], enzymes[19,20], GFP[21], IgG[22], cytokines[23]). Selected Nanofitins show many advantages compared to monoclonal antibodies: pharmacokinetic improvement for imaging, due to their small size; thermal stability, due to their origin; ease of in vitro production and scalability by bacterial expression systems. Thanks to these features, they represent versatile tools for diagnosis and therapy as with an anti-EGFR Nanofitin developed as PET radiotracer and a Nanofitin-based biotherapeutic agent directed against complement C3 (APL10-30), respectively[24,25].

In this work, an internalizing anti-HER-2 Nanofitin (NF), selected for its high specificity and affinity to HER-2 was produced to obtain large lots.

The purified protein was conjugated with the fluorophore IRDye800CW leading to a fluorescence derivative (NF-800, hereafter) for an in vitro/in vivo proof of concept by optical imaging (OI). IRDye800CW, as other near infrared (NIR) fluorophore family members with an excitation peak at 778 nm and an emission peak at 794 nm, presents minimal autofluorescence from biological samples, reduced light scattering and high tissue penetration, thus rendering it a fluorophore widely used in preclinical OI applications[26]. Binding and internalization properties of NF-800 were investigated, using high and low HER-2 expressing cells, to assess its specificity and labelling efficiency as well as the ability to compete with the monoclonal antibody Trastuzumab for the binding site.

Finally, in vivo administration at the dose of 10 nmol/mouse, in xenograft, orthotopic and patient-derived xenograft (PDX) tumor models, allowed to evaluate its biodistribution and tumor-targeting efficacy.

Results

Discovery and identification of NF, an internalizing anti-HER-2 Nanofitin

To identify affinity ligands specific to recombinant HER-2, Nanofitin libraries underwent 4 to 5 rounds of ribosome display against the recombinant human HER-2-Fc chimera protein, employed as bait. A total of 5×96 clones isolated from the resulting Nanofitin pools, enriched for binders, were screened as green fluorescent protein (GFP) fusions in crude bacterial lysis supernatant using ELISA (Fig. 1a). This screening unveiled several candidates of interest exhibiting a specific ELISA signal in the presence of the immobilized target, including NF.

Further screening identified 15 hits having novel sequences, high expression levels from bacterial fermentation, and specific affinity for HER-2 based on ELISA signal. After determining affinity as GFP fusions using biolayer interferometry (BLI) against immobilized HER-2-Fc chimera protein (not shown), the GFP was removed from the 5 candidates with the highest affinities for further characterization. Among these, NF was identified as the best candidate, and only its results are presented. Viability assays on high-expressing HER-2-(SK-BR-3)[27,28]and low-expressing (MCF-7)[27] cells demonstrated that NF effectively internalized and delivered the Pe38 toxin inside SK-BR-3 cells, with an EC_{50} of 0.83 nM, measured as NF-Pe38 fusion (Fig. 1b). In contrast, an irrelevant Nanofitin was unable to induce cell toxicity under the same conditions. Notably, MCF-7 cells exhibited decreased viability at higher concentrations with both NF and irrelevant Nanofitin, suggesting an intrinsic cellular response rather than specific internalization.

The sequence of the protein NF was, then, modified by introducing a cysteine residue at the C-terminal (NF-Cys), strategically placed to enable site-specific conjugation to a fluorophore. This modification was implemented with the goal of achieving a 1:1 conjugation ratio, ensuring precise labeling for downstream applications. Notably, no other cysteine residues are present in the protein structure, which eliminates the risk of non-specific

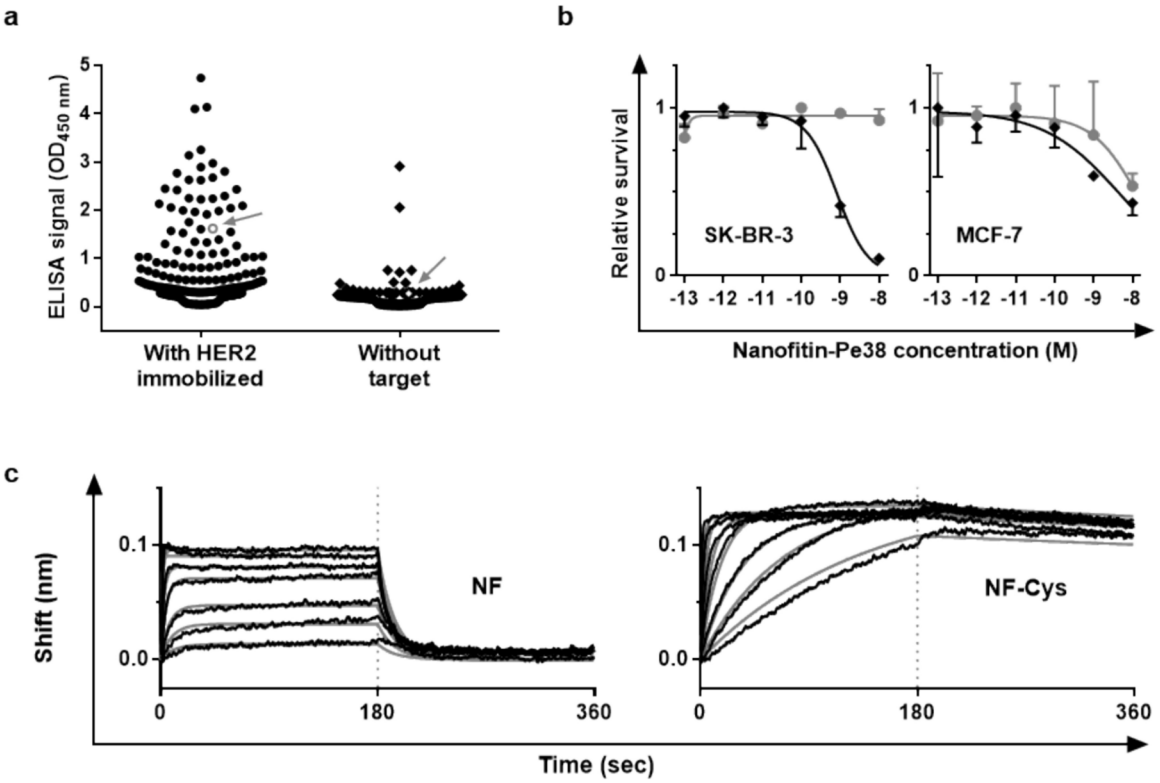

Fig. 1. Screening characterization leading to the identification of NF-Cys. (**a**)**,** Enzyme-linked immunosorbent assay (ELISA) screening for HER-2 ligands. Optical density at 450 nm (binding signal) measured in the presence or absence of immobilized HER-2 were determined for each Nanofitin clone fused to the green fluorescent protein. NF is highlighted in white and indicated by a gray arrow (NF-GFP). (**b**)**,** Measurement of SK-BR-3 and MCF-7 cells viability after incubation with the Pe38 toxin fused to either NF (NF-Pe38, black) or an irrelevant Nanofitin (gray) fused to the Pe38 toxin (n = 3, mean ± SD). (**c**)**,** Determination of the binding kinetics of NF before (left) and after (right) addition of a C-terminal cysteine, assessed by BLI on human HER-2. Fittings are represented as solid gray lines.

conjugation and allows for highly controlled and reproducible fluorophore attachment. As a consequence, the presence of a single cysteine determines the dimerization of the non-conjugated protein in oxidative conditions.

The affinity of NF and NF-Cys for the receptor was determined using BLI against immobilized HER-2-Fc chimera protein (Fig. 1c). The binding kinetics revealed affinities in the nanomolar range, with an avidity phenomenon for NF-Cys, resulting in its slower dissociation due to dimerization via a disulfide bridge in solution (NF: $K_D = 58.0$ nM; $k_{on} = 1.2 \times 10^6$ M^{-1} s^{-1}; $k_{off} = 70.5 \times 10^3$ s^{-1}; NF-Cys: $K_D = 0.9$ nM; $k_{on} = 0.5 \times 10^6$ M^{-1} s^{-1}; $k_{off} = 0.4 \times 10^3$ s^{-1}).

Nanofitin production and functionality evaluation

The protein was produced in transformed *E. coli* cells using induction with IPTG. Following bacterial lysis, protein purification was made in two steps: IMAC to purify the protein from residual DNA and the majority of contaminants[24], and SEC for the elimination of aggregates, monomers, and small contaminant proteins. Four different lots were produced with purity > 95% by IEX and SE-HPLC (Fig. S1). Notably, the non-reduced sample (panel a) showed small shoulders, suggesting the presence of a monomeric form. This suggestion was reinforced by the absence of these shoulders in the reduced sample and by the overlapping of the retention time of the cited shoulder with the reduced protein in panel b.

The four lots were also tested for functionality by ELISA assay showing K_D values in the single-digit nanomolar range (Table S1), as expected upon formation of an intermolecular disulfide bridge via its accessible cysteine residue, in accordance with BLI results. Of note, following conjugation with IRDye800CW, the Nanofitin NF-800 retained a nanomolar affinity in the double-digit range for the protein target (24.2 ± 9.7 nM), aligning with the expected affinity of NF in its monomeric state.

ELISA assay was also used to test the stability of NF-Cys (Lot 2820006) up to one year in eight different storage conditions, considering all the possible combinations relative to the following variables: two buffers (PBS and Protein Stability Cocktail or PSC), two storage temperatures (+ 2–8 or −20 °C), two concentrations (3 or 12 mg/mL). The fluctuations between time points for each condition did not appear statistically relevant and were attributed to experimental variability (Fig. S2). To capture differences, the analysis was simplified to means of each parameter during time. Overall, no statistical difference was observed between the storage

conditions for buffers and concentration. However, a statistically significant difference was revealed between temperatures: + 2–8 °C showed a lower K_D compared to −20 °C storage condition with $p < 0.05$. (Table S2).

Evaluation of NF-800 affinity for HER-2 expressed on cell surface and cell internalization

In order to carry out the full characterization of the conjugate NF-800, BT-474 and OE-19 were chosen as high expressing, whereas MCF-7 and HT-29 as low HER-2 expressing cell lines, according to literature data[27–29] (Figure S3 and Table S3). Both BT-474 and OE-19 cell lines were incubated with increasing concentrations of NF-800 to determine the affinity of the molecule for the cellular target.

NF-800 showed an *in cell* affinity similar to the abovementioned values obtained on the protein target, despite the greater complexity of the tested system, exhibiting a K_D value estimated at 53 ± 15 nM on BT-474 cells and 112 ± 12.3 nM on OE-19 cells, respectively. Distinct values for the two cell lines were due to the different contribution of the nonspecific signal, not measured in this experimental setting.

An important parameter to be evaluated on a new imaging agent is its internalization into the targeted cells. To this aim, NF-800 and the unconjugated dye IRDye800CW were subsequently incubated at either endocytosis-permissive or blocked temperatures (37 °C and 4 °C, respectively) on OE-19 and HT-29 cells. The internalization percent was derived from the percentage difference of the cell-associated fluorescence at 37 °C and 4 °C. As a result, NF-800 displayed the capacity to discriminate between high- and low-expressing cells and a considerable degree of internalization in OE-19 cells (about 90%) with a large advantage over the unconjugated dye IRDye800CW, used as control of non-specific uptake (Fig. S4).

In vitro competition with Trastuzumab and Pertuzumab for the binding site

A competitive ELISA was developed to test the ability of the Nanofitin NF-Cys to compete with the two monoclonal antibodies Trastuzumab (Tz) and Pertuzumab (Pz).

Briefly, a coated plate with HER-2 recombinant protein was incubated with variable concentrations of biotinylated antibodies in presence of high concentration of NF-Cys (at least 7.5-fold excess).

The curves of NF-Cys (Fig. 2a, b, squares) had a negligible decrease when Trastuzumab-biotin or Pertuzumab-biotin concentrations were increased (Fig. 2a, b, circles indicate the corresponding binding curves for the tested antibody). Moreover, curves of both antibodies were superimposable if tested in presence or in absence of NF-Cys (Fig. 2c, d). Overall, these results indicate that the epitope recognized by NF-Cys is separate and distinct from the epitopes recognized by Trastuzumab and Pertuzumab monoclonal antibodies. In fact, NF-Cys retained the binding properties to HER-2 and its specificity for the receptor was not affected by the presence of the two reference antibodies.

Competition for HER-2 binding site was also investigated on OE-19 cells. NF-800 at a saturating concentration (0.156 µM) and Trastuzumab conjugated with Alexa-488 (Tz-488) were incubated alone or in combination with a variable excess of the antibody (0.1 – 1 – 2 – 4 × with respect to the NF-800 concentration). The analysis was performed by acquiring both fluorophores. As shown in Fig. 2e, the binding of NF-800 to HER-2 expressed on the cell surface was unaffected by co-administration with an excess of Tz-488, indicating that they do not share the same binding site. In parallel, the binding extent of the antibody was different only for the sample with a 0.1 × excess of Tz-488 (Fig. 2e, f), a non-saturating concentration of the antibody on cell lines (data not shown).

In vivo studies

To test the imaging performance of NF-800 in visualizing HER-2-expressing tumors, in vivo experiments were performed on different tumor models.

The in vivo biodistribution of NF-800 was observed at different time points up to 48 h after the injection in a BT-474 xenograft tumor model (Fig. S5). Muscle was selected as the background healthy tissue for contrast evaluation in the lesions. NF-800 showed a significantly higher localization in tumor than in muscle already at early time points, reaching a tumor-to-background (TBR) of 2.09 ± 0.66 at 6 h after injection, which remained constant up to 48 h (Fig. 3a). The kinetic optical imaging acquisitions of animals also showed the localization of NF-800 in kidneys and liver, that was confirmed by ex vivo analysis on excised tissues. At 6 h a higher signal in liver and kidney than in tumor was observed. At 24 and 48 h, the fluorescence signal slightly decreased in tumor and in liver whereas a drastic increase of signal was observed in kidney (Fig. 3b). In terms of TBR, the ratiometric evaluation showed a significant increase in kidney values over time ($p = 0.00005$, Turkey's multiple comparison test) with respect to the liver contrast, as a demonstration of the predominant renal excretion pathway of NF-800. In tumors the TBR slightly increased (27.2%) up to 48 h (Fig. 3c).

The BT-474 results were, then, compared to those obtained in HER-2 low-expressing tumor models, *i.e.* in MCF-7 and HT-29 xenograft tumor bearing mice. NF-800 was administered and animals were sacrificed at 24 h and 48 h post-injection. In both cases a significantly higher ex vivo TBR was observed for BT-474 tumors (7.5 ± 1.8 and 7.7 ± 1.2) than in MCF-7 tumors (3.7 ± 0.5) at 24 h ($p = 0.0053$, Unpaired t test) and HT-29 tumors (4.8 ± 1.1) at 48 h ($p = 0.0141$, Unpaired t test), demonstrating a substantially higher accumulation of NF-800 in HER-2 high expressing tumors (Fig. S6).

Being OE-19 an alternative cell line characterized by high HER-2 expression, the specificity of NF-800 to the target was further validated on the OE-19 xenograft model. Here, NF-800 showed remarkably higher fluorescent contrast compared to the BT474 xenograft model (ex vivo TBR value of 11.1 ± 3.1 *vs* 5.3 ± 1.3 at 6 h post-administration; data not shown). This observation was also confirmed in orthotopic OE-19 tumors at the same time of sacrifice (*i.e.*, 6 h). In this model, in the ex vivo acquisition the fluorescent signal of NF-800 was primarily observed in the tumor with respect to the surrounding area (*i.e.,* stomach and oesophagus, as showed in the Fig. 4a, where the asterisk indicates the location of the tumour). Moreover, the mean TBR observed was 9.7 ± 3.4, significantly higher than the value obtained in BT-474 tumors (5.3 ± 1.3; $p = 0.0139$, Two-way ANOVA, Tukey's multiple comparisons test) (Fig. 4b). An exhaustive comparison of the ex vivo biodistribution in high

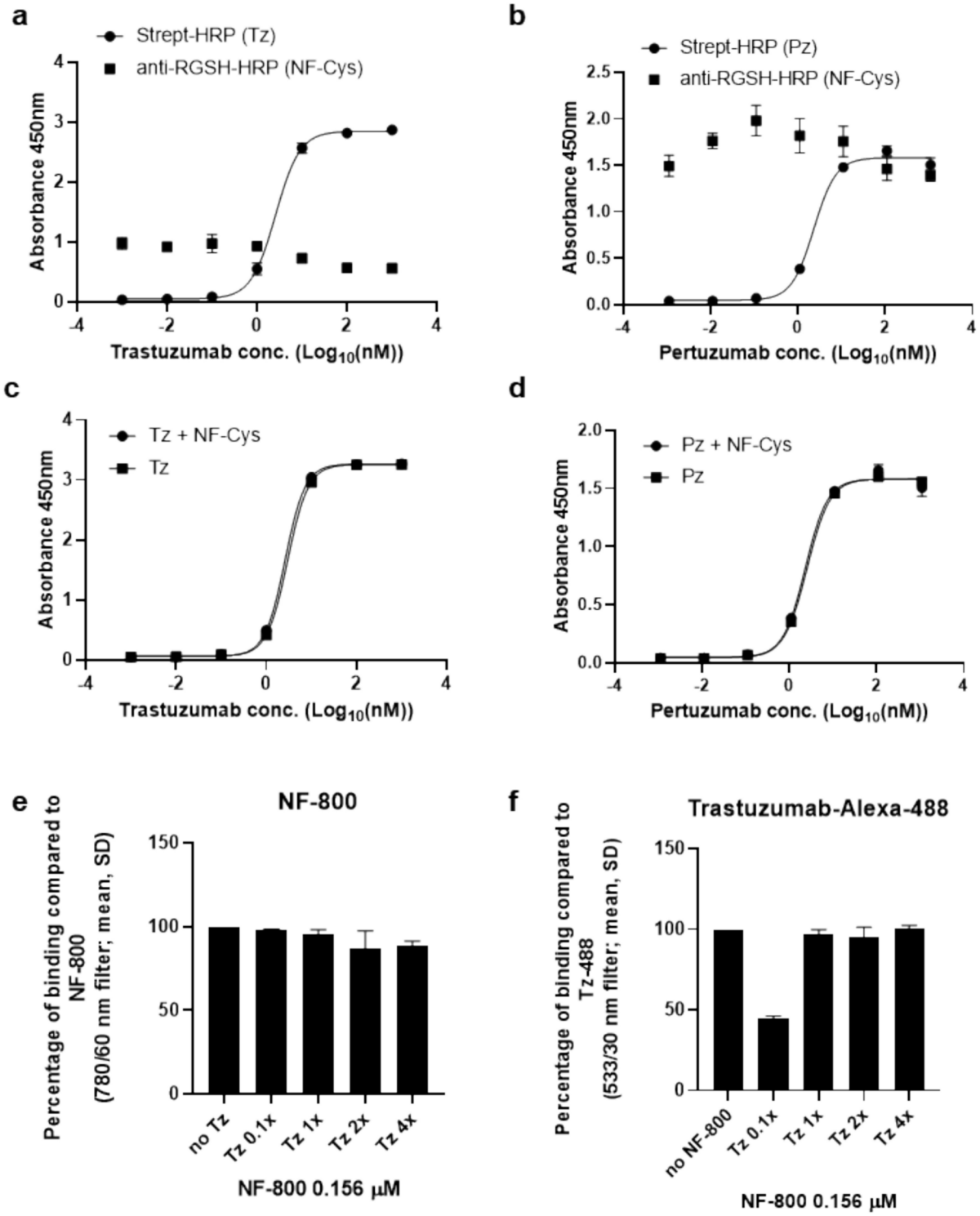

Fig. 2. Nanofitin competition analysis with Trastuzumab and Pertuzumab antibodies. (**a-d**), NF-Cys competition analysis with Trastuzumab and Pertuzumab for the binding site by competitive ELISA assay. (**a, b**), Duplicate plates were incubated with Streptavidin-HRP for antibody signal detection or with anti-RSGH Tag-HRP for Nanofitin signal detection. n = 2, mean ± SD. (**c, d**), Binding of Trastuzumab or Pertuzumab in presence or absence of NF-Cys. n = 2, mean ± SD. (**e, f**), NF-800 binding on OE-19 cells in presence of variable excess of Trastuzumab-Alexa-488. n = 2, mean ± SD. (**e**), Acquisition with flow cytometry setting on IRDye800CW wavelengths; (**f**), acquisition with flow cytometry setting on Alexa-488 wavelengths.

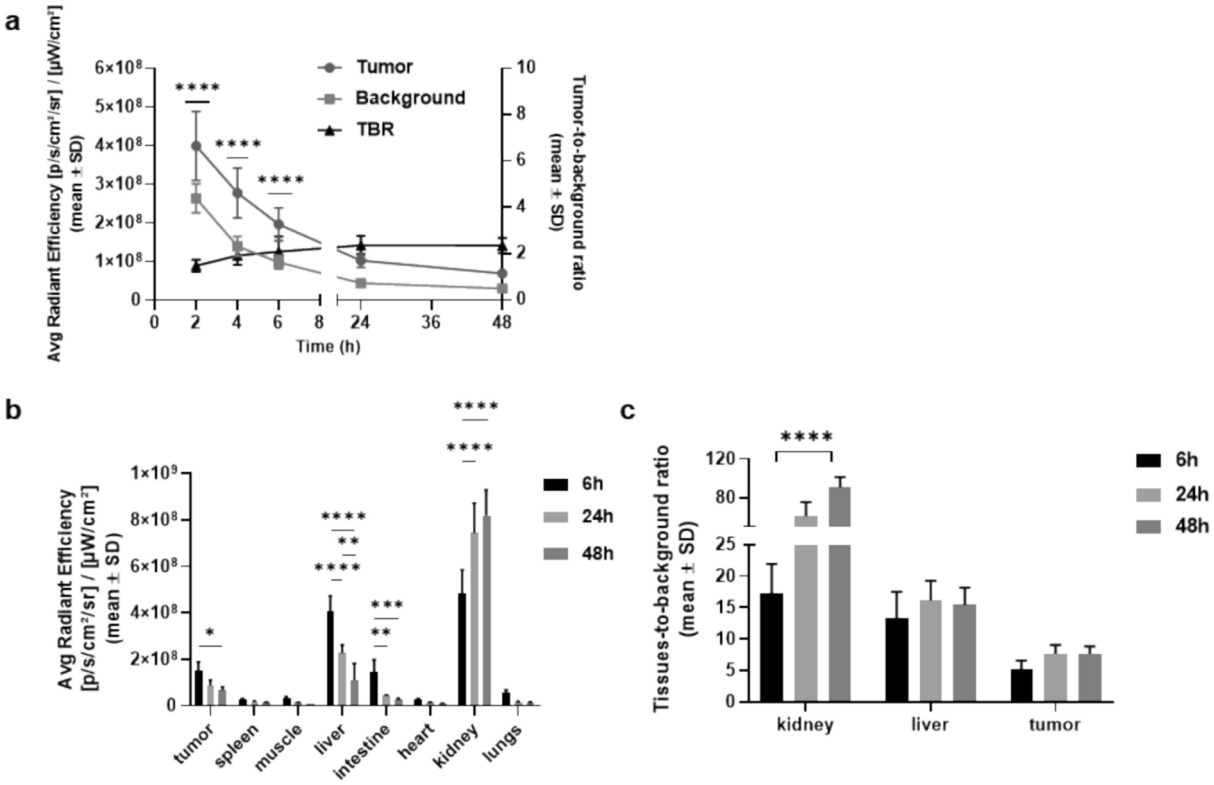

Fig. 3. In vivo and ex vivo biodistribution at different time points after administration of NF-800 in BT-474 xenograft tumor bearing mice. (**a**), In vivo fluorescence signal decay in tumor and muscle and TBR (mean ± SD). Two-way ANOVA, Sidak's multiple comparisons test (* = $p \le 0.05$; ** $p \le 0.01$; *** $p \le 0.001$; **** $p \le 0.0001$). (**b**), Ex vivo biodistribution in tumor and main organs. Results are expressed as Average Radiant Efficiency (mean ± SD). (**c**), Ex vivo tumor and excretory organs (liver and kidney) to background ratio. Two-way ANOVA, Tukey's multiple comparisons test (* = $p \le 0.05$; ** $p \le 0.01$; *** $p \le 0.001$; **** $p \le 0.0001$). For each group at least n = 4.

HER-2 expressing tumor models was shown in Fig. S7, where the probe selectively accumulated in the tumor mass if compared to healthy tissue. A high fluorescence intensity was also observed in the kidneys as well as in the liver, due to the mechanisms that regulates the excretion of NF at an early time point (6 h).

The efficacy of NF-800 was also compared to the anti-HER-2 Trastuzumab antibody in a similar experiment within the OE-19 orthotopic tumor model. The ex vivo TBR measured 6 h after administration of Trastuzumab-IRDye800CW (Tz-800) at the dose of 0.5 nmol/mouse was 5.1 ± 1.9, statistically lower than the value obtained with NF-800 ($p = 0.0034$, Two-way ANOVA, Tukey's multiple comparisons test) (Fig. 4c).

All tumor models were fully characterized in terms of HER-2 expression and vascularization in order to obtain a complete evaluation of the biodistributions results. Immunofluorescence of tumor sections confirmed BT-474 and OE-19 as high HER-2 expressing tumor. On the other hand, MCF-7 and HT-29 have been confirmed as being low HER-2-expressing tumors. The vascularization, estimated on the endothelium area, had a similar extent in the different types of tumors. This is an important evaluation when the specificity of a target molecule is to be evaluated in different pathological models. Differences in the vascular area might lead to misleading interpretation and comparison of TBRs. However, this is not the case for the models selected in the frame of this work. All in all, these results suggest that the greater advantage of NF-800 in HER-2 tumor retention is largely due to this differential target expression (Fig. S8 and Table S4), as discussed above.

Finally, the potential of NF-800 as a HER-2 targeted fluorescent probe was also investigated in a PDX model (Fig. S9) derived from metastatic colorectal cancer selected for HER-2 overexpression (Table S5 and Fig. S10). The NF-800 tumor-targeting properties were compared with the anti-HER-2 Trastuzumab antibody. This evaluation was performed by comparing TBR for the two compounds acquired at their maximum expected signals in this model, 24–48 h for NF-800 and 7 days for Trastuzumab. Indeed, antibodies are characterized by a long blood residence time, and hence by a delayed optimal imaging windows with respect to small molecules[30].

The ex vivo TBR obtained at 48 h for NF-800 and 7 days for Tz-800 was 3.3 ± 0.7 and 2.4 ± 0.1, respectively. These data demonstrated that, even if the contrast in the PDX model was analyzed at longer time points (48 h) compared to other HER-2 high expressing models, the obtained value was always significantly higher than the contrast found with the anti-HER-2 antibody Trastuzumab at its optimal window acquisition (Fig. 5).

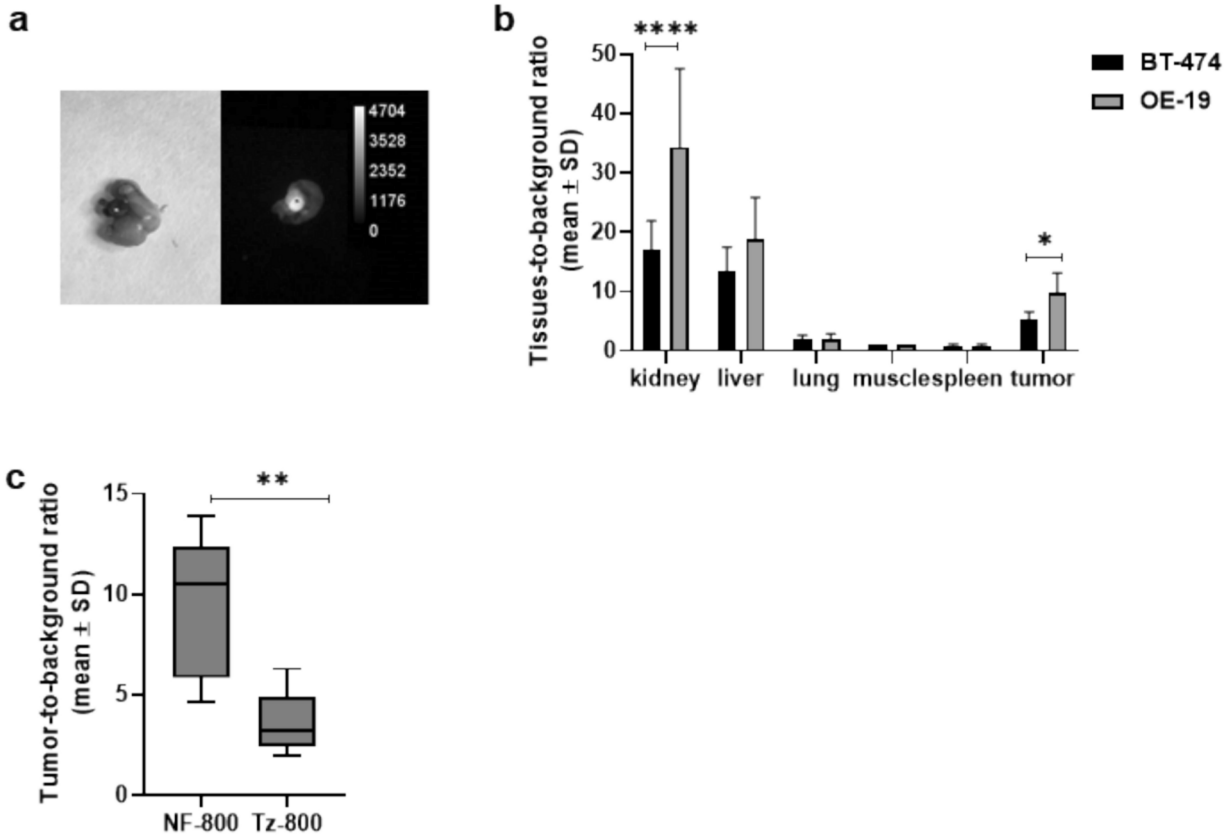

Fig. 4. Ex vivo analysis of NF-800 efficacy in OE-19 orthotopic tumor bearing mice 6 h after administration. (**a**)**,** Ex vivo photograph and fluorescence intensity image of OE-19 orthotopic tumor model after *i.v.* administration of NF-800 (Asterisks indicate the tumor in both images). (**b**)**,** Ex vivo comparison analysis of NF-800 biodistribution in BT-474 xenograft and OE-19 orthotopic tumor bearing mice. (**c**)**,** Comparison of the ex vivo efficacy of NF-800 (10 nmol/mouse) *vs* Tz-800 (2.5 mg/kg) in OE-19 orthotopic tumor model. Data are expressed as tumor-to-muscle ratio (Mean ± SD). For each group at least n = 5.

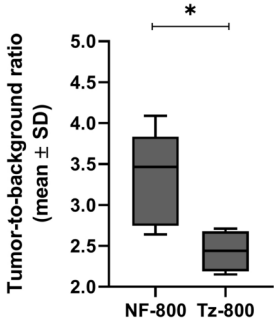

Fig. 5. Comparison of the ex vivo efficacy of NF-800 (10 nmol/mouse, n = 6) *vs* Tz-800 (2.5 mg/kg, n = 4) in PDX tumor model 48 h and 7 days after injection, respectively. Data are expressed as tumor to muscle ratio (For each group at least n = 4; mean ± SD).

Discussion

An ideal diagnostic tool for cancer imaging must combine fast elimination, high uptake and specific tumor targeting in order to show a clear and distinguishable signal shortly after administration.

HER-2 has been widely accepted as a relevant target for cancer therapy, but the need for the non-invasive detection of HER-2 associated tumors is still an open question, especially during therapy. In fact, limitations of antibodies for diagnostic and therapy monitoring purposes have stimulated research towards smaller, faster excreted probes[31].

In the present work, we developed the truly innovative targeting agent NF-800, with a suitable pharmacokinetics profile specifically designed for non-invasive diagnostic purposes. NF-800 was developed

exploiting the Nanofitin molecular vector platform. The probe is characterized by a high expression yield, and specific binding and internalization properties directed towards HER-2.

To the best of our knowledge, this is the first HER-2 targeted agent specifically developed for diagnostic purposes in the field of OI, that might also be used to monitor (non-invasively) the early response to therapy with HER-2 targeted antibodies. The great advantage is to provide early evidence of tumor response with high resolution and sensitivity, so that alternative treatment options can be initiated, in case of treatment resistance, or long-term efficacy can be predicted. To date, a wide variety of radiopharmaceuticals had been made available in clinical practice to evaluate the biological features of tumors. Among these probes, ^{18}F-FDG for tumor metabolism, ^{18}F-FMISO for hypoxia, ^{18}F-FLT for tumor cell proliferation, ^{18}F-labeled amino acids for protein synthesis, and ^{15}O–water for blood flow can be mentioned[32]. They give, however, a generic evaluation to the response to cancer treatment. On the other hand, there are several tracers that have been specifically developed for the evaluation of downregulation of HER-2 in targeted therapy, such as antibodies, shorter fragments (*i.e.*, antibody fragments, diabodies, affibodies), and small molecules[33]. However, they have been developed for nuclear medicine applications[32,34–36], with only few of them specifically designed to monitor response to Trastuzumab[37–39], a standard-of-care molecule. Of note, none of these probes has reached approval.

Not only NF-800 has been specifically designed for OI applications, but it can also be used in Fluorescence Guided Surgery (FGS) to help clinicians to remove primary lesions and assess lymph node involvement. FGS in oncology might be helpful in delineating tumor margins, but it requires tumor-specific optical guide able to selectively bind to tumoral tissue: OTL38 (Cytalux), a fluorescent agent which enhances the intraoperative localization of difficult-to-identify ovarian and lung cancer tissues, has been recently approved by FDA[40,41].

NF-800 is hence a pluripotent targeted agent that can be adapted in many clinical onsets.

Biodistribution and tumor targeting specificity of NF-800 were evaluated firstly in vitro and then in xenograft, orthotopic and patient-derived xenograft (PDX) tumor models overexpressing HER-2.

This extensive characterization of NF-800 demonstrated the validity of this molecular imaging probe in terms of specificity, tumor detection and optical imaging performance.

In vivo and ex vivo, NF-800 displayed a low signal in all non-excretion organs (*i.e.*, all organs excluding liver, kidneys and intestine), while a high fluorescent signal was found in HER-2 expressing tumors. The NF-800 signal was also found to be high in kidneys at all timepoints and in liver 6 h post injection. While the high signal in the liver at the earliest timepoint is most likely to be related to the extensive parenchymal vascularization of the hepatic tissue, the predominant nephric biodistribution at 24 h suggests a preferential renal excretion route of the construct[24,42]. This kind of drug elimination (including a high signal in liver shortly after administration, that decreases at later imaging timepoints) is common for small molecules, as reported in other OI applications[43,44], and brings several advantages for both imaging and surgery applications. In particular, it could minimize the potential hazards to normal tissues and healthy organs in radiolabeling diagnosis, but also allow a rapid tumor targeting[24,45], which results in short hospital residency time (*i.e.* a few hours) for patients between administration of the contrast agent and time of imaging. Indeed, BT-474 tumors overexpressing HER-2 were clearly delineated already at 6 h after injection in time-dependent optical imaging acquisitions with an ex vivo TBR constant until 48 h. Comparing results with two HER-2 low expressing tumor models, NF-800 showed a significantly higher uptake in BT-474 with respect to MCF-7 tumors at 24 h and HT-29 tumors at 48 h, demonstrating the receptor-specificity of NF-800, as already assessed in vitro.

The tumor targeting efficacy was also confirmed in two translational preclinical cancer setups, as OE-19 orthotopic tumors, and a patient-derived xenograft (PDX) model, where NF-800 targeting efficacy was compared to the anti-HER-2 antibody Trastuzumab. In both models, NF-800 showed a large advantage with respect to Trastuzumab, especially at earlier time points, in light of the delayed optimal window acquisition characterizing antibodies due to their prolonged blood residence time. Most importantly, from in vitro competition experiments, NF-800 did not seem to share the same binding site with the therapeutic antibodies Trastuzumab and Pertuzumab. All the above-mentioned results are coherent with the in vitro findings for specificity and efficacy acquired on NF-800.

This finding is of paramount importance since it opens up the possibility of using NF-800 as a diagnostic tool to monitor early therapeutic response in patients referred to treatment with Trastuzumab and Pertuzumab, and to use NF-800 for FGS in patients that underwent neoadjuvant therapy with targeted antibodies before surgery.

The future scalability of the probe was explored by investigating its production and its purification steps. The upstream production of the NF-Cys proved to be robust and scalable. The downstream purification was successfully achieved and can be confidently forecasted to scale up effortlessly. The purified protein demonstrated to be stable over time and successfully conjugated to IRDye800CW without major alterations of its affinity for the protein target. These findings suggest its suitability for reliable use in diagnostic applications within the field of oncology. Moreover, they underscore the ability of the Nanofitin technology to maintain its binding activity while conjugated with other imaging reporting agents, such as PET tracers[24].

In conclusion, these results pave the way to the clinical development of NF-800 as a tool able to help in non-invasive detection of HER-2 associated tumors, patient stratification, therapy efficacy monitoring and even in image-guided surgery applications.

Methods

Generation and identification of anti-HER-2 Nanofitin NF

Nanofitins were generated by ribosome display selection against recombinant human ErbB2/HER-2 Fc chimera proteins (1129-ER, R&D Systems) from naïve 14-position libraries[18]using multiple rounds of selection as previously described[21,25], using non-biotinylated proteins immobilized on Sera-Mag SpeedBeads Protein A/G magnetic particles (17152104010150, Thermo Scientific). Screening of Nanofitins affine for HER-2 was performed by measuring ELISA signal against immobilized antigen with Nanofitins fused to the green

fluorescent protein, as previously described[25]. Screening of internalizing Nanofitins was performed by measuring cell viability of SK-BR-3 (HTTB-30, ATCC) and MCF-7 (HTB-22, ATCC) cells after incubation with Nanofitins fused to the Pe38 toxin domain as previously described[24]. Binding kinetics were initially evaluated by biolayer interferometry (BLI), by simultaneously exposing the HER-2-Fc chimera protein immobilized on biosensors to various concentrations of Nanofitins (1000, 500, 125, 62.5, 31.3, 15.6, and 0 nM), as previously described[45]. The anti-HER-2 Nanofitin identified during screening is referred to as NF, NF-GFP, or NF-Pe38, depending on its fusion format: untagged, fused to green fluorescent protein, or fused to the Pe38 toxin domain, respectively. The anti-HER-2 hit, modified with a C-terminal cysteine (NF-Cys) and subsequently conjugated to IRDye800CW (NF-800), is described in dedicated sections below.

Nanofitin NF-Cys

Nanofitins NF-Cys is an 8674 Da (monomer) protein. It shows a single cysteine at C-terminal for site-specific conjugation and an RGS/histidine tag (complete sequence RGSHHHHHH) at N-terminal[46], exploited for both selection step and ELISA assay. The presence of a single cysteine determines the dimerization of the protein in oxidative conditions.

The molar extinction coefficient and pI were calculated from the primary sequence of the recombinant protein using an online software (https://web.expasy.org/protparam/). Nanofitin NF-Cys shows a low theoretical molar extinction coefficient (2980 M-1 cm-1 at 280 nm) and a pI of 7.96.

Nanofitins production and purification

Nanofitins expression and purification were carried out at different scales in the discovery and characterization process: 200 ml for small scale or 3000 ml using a shaking flask, with the protocol described by Goux *et al*[24].

A further purification step with respect to literature was carried out to improve the purity of the Nanofitin.

The fractions containing the purified Nanofitin NF-Cys were pooled and concentrated up to 4 mL in ultrafiltration cell equipped with a 3000 Da MWCO membrane.

The concentrated protein solution was applied into a SEC column (Sephacryl S-100 HR, 16 × 600 mm, Cytiva) previously equilibrated with PBS. The elution was performed with PBS at 1 mL/min.

The fractions containing the purified Nanofitin NF-Cys were pooled together and filtered in sterile conditions on a 0.22 µm membrane.

Final concentration was determined by UV–Vis (Lambert–Beer Law) using a molar extinction coefficient of 2980 M^{-1} cm^{-1} at 280 nm.

HPLC analysis

Two HPLC methods were applied to analyze the purified NF-Cys: ion exchange (IEX) and size exclusion (SE).

Purified product analysis was carried out by HPLC analysis (1260 HPLC, Agilent) using a size exclusion column (Zenix-C SEC-80 4.6 × 300 mm, Sepax). A 0.1 M sodium phosphate, 0.15 M NaCl, pH 7.0 + 10% Acetonitrile buffer was used as mobile phase with a constant flow of 0.35 mL/min and the system was run isocratically at 30 °C. The product was detected with an UV detector at 280 nm.

Reduction reaction was evaluated with an IEX-HPLC method using a ProPac WCX-10 4 × 250 mm (Thermo) column. A gradient from 20 mM TRIS pH 7.5 + 10% Isopropanol to 20 mM TRIS, 1 M NaCl, pH 7.5 + 10% Isopropanol was run in 10 min at 30 °C with a constant flow of 1 mL/min. The eluted proteins were detected with a UV detector at 230 and 280 nm.

Nanofitin conjugation to IRDye800CW-maleimide (NF-800)

The reduction of the cysteine was performed 1 h at room temperature using a 35-fold molar excess of TCEP compared to the protein. Complete reduction of the protein was tested by IEX-HPLC analysis. Then, IRDye800CW-maleimide (LI-COR) was added in excess (molar ratio dye-maleimide:nanofitin 3:1), and the reaction was allowed to proceed for 5 h. The conjugation mix was applied into a SEC column (Sephacryl S-100 HR, 16 × 600 mm, Cytiva) previously equilibrated with PBS, to remove the fluorescent dye excess. The elution was performed with PBS at 1 mL/min.

The fractions containing purified Nanofitins NF-800 were pooled together and filtered in sterile conditions on a 0.22 µm membrane.

Final concentration was determined by UV–Vis (Lambert–Beer Law) using the molar absorption coefficient of IRDye800CW, ε = 240,000 M^{-1} cm^{-1} (at 780 nm).

ELISA assay

Screening assay

The ELISA assay was performed as described by Mouratou *et al*[46].

Binding assay

The protocol was adapted by Mouratou *et al*[46]. MaxiSorp 96-well plates were coated with HER-2 Fc chimera protein (R&D systems) at 2.5 µg/mL in TBS 1X (TRIS 20 mM, NaCl 150 mM) Nanofitin samples were incubated three-fold serially diluted to give concentration ranges from 1.35 to 6.17E-04 µM in duplicates. Plates were read at 450 nm on a Spark multimode microplate reader (Tecan) using SparkControl software v2.3. Coated wells were also read without prior incubation with Nanofitin NF-Cys and antibody to measure blank. Results were analyzed by non-linear regression method with a one-site binding model using GraphPad Prism 8 software to determine Bmax and K_D.

Competitive ELISA assay

To perform the competitive ELISA assays, Trastuzumab and Pertuzumab were conjugated with biotin PEG4-NHS. Briefly, 10 mg of each antibody was diluted to 5 mg/mL with PBS and added of 250 µL of 1 M Sodium Phosphate, pH 9.0. EZ-Link NHS-PEG4-Biotin, 21 µL of a 10 mg/mL solution in DMSO, was added to the antibody. The reaction was performed for 2 h at room temperature. At the end of the incubation, the conjugated protein was purified by Zeba Spin Desalting Columns, 7 K MWCO, using PBS as eluent. The final concentration was determined by UV/Vis (Lambert–Beer Law) using a molar absorption coefficient ε = 215,380 M-1 cm-1 (at 280 nm) for Trastuzumab (MW 145,401 g/mol) and ε = 210,340 M^{-1} cm^{-1} (at 280 nm) for Pertuzumab (MW 145,332 g/mol).

Different concentrations of Trastuzumab-biotin or Pertuzumab-biotin (1000, 100, 10, 1, 0.1, 0.01 and 0.001 ng/mL) were incubated together with a saturating concentration of NF-Cys (10 µg/mL) in each well in duplicate (1 h at RT) in TBS + 0.1% Tween 20 (TBS-T). As control, both antibodies concentration ranges were also incubated in absence of NF-Cys.

At the end of the incubation, the plate was washed three times with TBS-T and incubated with Streptavidin-HRP 1:10,000 for antibody signal detection, or in alternative with anti-RGSHis Tag-HRP 1:4000 in TBS-T (1 h at RT) for Nanofitin signal detection.

One-year stability test

Nanofitin NF-Cys was stored in two different buffers (PBS and Protein Stability Cocktail or PSC, Thermo Fisher Scientific), each buffer at two temperatures (+ 2–8 °C and −20 °C) and two different concentrations (3 and 12 mg/mL), for a total of 8 different samples. Analyses were performed every two months over one year evaluating the Nanofitin functionality by ELISA assay, as described previously.

Flow cytometry evaluation of binding affinity and competition with Trastuzumab

Human breast cancer cells BT-474, human colon adenocarcinoma cells HT-29 (ATCC) and human oesophageal carcinoma cells OE-19 (Sigma-Aldrich) were grown in DMEM F-12 medium, McCoy's 5A medium, or RPMI-1640, respectively. All media were supplemented with 10% FBS, 2 mM glutamine, 100 IU/mL penicillin and 100 µg/mL streptomycin.

For binding affinity evaluation, BT-474 and OE-19 cells were incubated with increasing concentrations (range 20 – 0.039 µM) of NF-800 for 90 min on ice in the dark. After incubation, cells were rinsed repeatedly in cold Flow Cytometry Staining Buffer (Thermo Fisher Scientific), centrifuged and cell pellets were, then, resuspended in cold Flow Cytometry Staining Buffer to be analyzed with the flow cytometer Accuri C6 (BD Biosciences). The mean cell-associated fluorescence was plotted against concentration and the dissociation constant at equilibrium (K_D) was inferred by mathematical fitting with GraphPad Prism v.9 software (One site – Total).

In competition experiments, NF-800 0.156 µM and Trastuzumab-Alexa-488 0.625 µM (R&D Systems) were incubated alone or in combination with an excess of Trastuzumab-Alexa-488 (0.1 – 1 – 2 – 4x) in the same treatment buffer. Co-incubated samples were acquired with filters specific for each fluorophore (780/60 nm filter for IRDye800CW and 533/30 nm filter for Alexa-488). Results were expressed as percentage of binding with respect to the only treatment with Nanofitin or the antibody (set to 100%).

Cellular uptake assessment by flow cytometry

NF-800 or IRDye800CW were incubated 1 µM in serum-free medium with 25 mM HEPES pH 7.4 on plated cells for 2 h at 37 °C or on ice in the dark. At the end of treatment, cells were washed with cold PBS and detached from the plate. Cell suspension was diluted in cold PBS and centrifuged. The cell pellet was resuspended in cold Flow Cytometry Staining Buffer. Results were expressed as normalized cell-associated fluorescence intensity (FI), calculated with the following formula:

$$Normalized\ FI = \frac{(FI_{treated\ sample} - FI_{untreated\ sample})}{FI_{untreated\ sample}} \quad (1)$$

In vivo studies

BALB/c nu/nu mice (Charles River Laboratories and Envigo RMS) were inoculated with BT-474 (n = 12), MCF-7 (n = 4), HT-29 (n = 4) or OE-19 (n = 7) cell suspension to obtain xenograft tumors. At the time of the tumor inoculation, the mice were 5–7 weeks old and had body weights of 16.5 ± 1.6, 16.5 ± 1.2, 18.7 ± 0.8, and 23.5 ± 1.5 g, respectively (mean ± SD). For BT-474 and MCF-7, three or fifteen days before cell inoculation, a pellet containing 17β-estradiol (Innovative Research of America) was implanted to help the subsequent development of the tumors. BT-474 were, then, inoculated in the presence of Matrigel. Cell suspension was subcutaneously injected in the right flank in general gas anesthesia by using 5–6% sevoflurane. After inoculation tumors development was followed twice a week by palpation and caliper measurement.

For the orthotopic model, OE-19 xenograft tumor fragments were sutured on the esophageal serosa of athymic nude mice (n = 10) (Envigo RMS), following the Gros et al.procedure[47], and tumor development was followed by MRI acquisitions (PharmaScan 7 T scanner). At the time of the orthotopic tumor implantation, the mice were 10 weeks old and had body weights of 24.7 ± 1.6 g (mean ± SD).

All procedures involving animals were performed in accordance with national and international laws on the.

use of experimental animals (L.D. 26/2014; Directives 2010/63/EU) under the Ministerial Authorizations (project Research Number: 46/2015-PR; 329/2019-PR; 478/2021-PR; 543/2022-PR) and in accordance with the ARRIVE guidelines.

PDX model

Sixteen NOD-SCID mice were inoculated in a subcutaneous pocket on the right flank with human tumor tissue fragments (PDX) derived from a metastatic colorectal tumor characterized by amplification (accompanied by strong over-expression) of the HER-2 gene[48] (ID CRC0080 in the Institute biobank). Tumor growth was monitored with a caliper twice a week until the predefined range of 220–400 mm^3 was reached. Tumor HER-2 and EGFR expression in PDX model was assessed by pathological examination. Further details are available in the Supporting Information section.

Animal procedures were approved by the Ethical Commission of the Candiolo Cancer Institute and by the Italian Ministry of Health. All patients provided informed consent, including for sex and age information collection. All methods were carried out in accordance with relevant guidelines and regulations. Samples were procured and the study was conducted under the approval of the Review Board of the Fondazione del Piemonte per l'Oncologia FPO—IRCCS (Profiling protocol No. 001-IRCC-00IIS-10, version 11.0, updated July 13, 2022).

Optical imaging (OI)

OI experiments on tumor bearing animals were performed after administration of NF-800 at a dose of 10 nmol/mouse or Trastuzumab-IRDye800CW 0.5 nmol/mouse. In vivo OI experiments were performed on the IVIS Spectrum system (Perkin Elmer) for the xenograft and the Explorer Air 1 prototype (SurgVision GmbH) for the orthotopic tumor models, respectively. During OI experiments animals were maintained under gas anesthesia.

Following in vivo OI experiments, tumor bearing mice were sacrificed and tumor and main organs were excised for ex vivo fluorescent signal measurement.

Image analyses were carried out using ImageJ open software (NIH) for the orthotopic tumor model, whereas IVIS Living Image Software was used to analyze the xenograft and PDX tumor models. Regions of interest (ROIs) were drawn on the tumor or on the organs and on a reference background healthy region (hind limb muscle) of the mouse for each fluorescence image at every time point to evaluate signal intensity in the tissues (expressed as Average Radiant Efficiency) (Fig. S11). The ratio between the fluorescence signal in the tumor or in the organs and background healthy tissue (TBR and OBR, respectively) was, then, calculated to assess the contrast.

Statistical analysis

Statistical analysis was performed using Prism software (GraphPad by Dotmatics) applying test indicated in the results.

Data availability

The datasets generated and/or analysed during the current study are not publicly available due Company's confidentiality policy but are available from the corresponding author on reasonable request.

Received: 26 June 2024; Accepted: 10 March 2025
Published online: 21 March 2025

References

1. Iqbal, N. & Iqbal, N. Human epidermal growth factor receptor 2 (HER2) in Cancers: Overexpression and therapeutic implications. *Mol. Biol. Int.* **2014**, 1–9 (2014).
2. Fukushige, S.-I. et al. Localization of a novel V-ErbB-Related gene, c-ErbB-2, on human chromosome 17 and its amplification in a gastric cancer cell line. *Mol. Cell. Biol.* **6**, 955 (1986).
3. Friedman, M. & Ståhl, S. Engineered affinity proteins for tumour-targeting applications. *Biotechnol. Appl. Biochem.* **53**, 1–29 (2009).
4. Ahn, S., Woo, J. W., Lee, K. & Park, S. Y. HER2 status in breast cancer: Changes in guidelines and complicating factors for interpretation. *J. Pathol. Transl. Med.* **54**, 34–44. https://doi.org/10.4132/jptm.2019.11.03 (2020).
5. Swain, S. M., Shastry, M. & Hamilton, E. Targeting HER2-positive breast cancer: Advances and future directions. *Nat. Rev. Drug Discov.* **22**, 101–126. https://doi.org/10.1038/s41573-022-00579-0 (2023).
6. Wolff, A. C. et al. Human epidermal growth factor receptor 2 testing in breast cancer: American society of clinical oncology/college of American pathologists clinical practice guideline focused update. *J. Clin. Oncol.* **36**, 2105–2122 (2018).
7. Zhang, H., Moisini, I., Ajabnoor, R. M., Turner, B. M. & Hicks, D. G. Applying the new guidelines of HER2 testing in breast cancer. *Curr. Oncol. Rep.* https://doi.org/10.1007/s11912-020-0901-4 (2020).
8. Gong, C. et al. Temporal heterogeneity of HER2 expression and spatial heterogeneity of 18F-FDG uptake predicts treatment outcome of pyrotinib in patients with HER2-positive metastatic breast cancer. *Cancers (Basel)* **14**, 3973 (2022).
9. Zhang, Q. et al. Temporal heterogeneity of HER2 expression in metastatic gastric cancer: A case report. *World J. Surg. Oncol.* https://doi.org/10.1186/s12957-022-02615-0 (2022).
10. Katayama, A. et al. Predictors of pathological complete response to neoadjuvant treatment and changes to post-neoadjuvant HER2 status in HER2-positive invasive breast cancer. *Mod. Pathol.* **34**, 1271–1281 (2021).
11. Petroni, S. et al. Fish testing of HER2 immunohistochemistry 1+ invasive breast cancer with unfavorable characteristics. *Oncol. Lett.* **12**, 3115–3122 (2016).
12. Fischman, A. J., Alpert, N. M. & Rubin, R. H. Pharmacokinetic imaging. *Clin. Pharmacokinet.* **41**, 581–602 (2002).
13. Lee, I. et al. A preliminary clinical trial to evaluate 64Cu-NOTA-trastuzumab as a positron emission tomography imaging agent in patients with breast cancer. *EJNMMI Res.* https://doi.org/10.1186/s13550-021-00746-1 (2021).
14. Mortimer, J. E. et al. Functional imaging of human epidermal growth factor receptor 2-positive metastatic breast cancer using 64Cu-DOTA-trastuzumab Pet. *J. Nucl. Med.* **55**, 23–29 (2014).
15. Luo, R., Liu, H. & Cheng, Z. Protein scaffolds: Antibody alternatives for cancer diagnosis and therapy. *RSC Chem. Biol.* **3**, 830–847. https://doi.org/10.1039/d2cb00094f (2022).
16. Shi, J. et al. Molecular imaging of HER2 expression in breast cancer patients using a novel peptide-based tracer 99mTc-HP-Ark2: A pilot study. *J. Transl. Med.* https://doi.org/10.1186/s12967-022-03865-y (2023).
17. Cai, J. et al. Non-invasive monitoring of HER2 expression in breast cancer patients with99m TC-affibody SPECT/CT. *Iran. J. Radiol.* https://doi.org/10.5812/iranjradiol.96419 (2020).

18. Mouratou, B. et al. Remodeling a DNA-binding protein as a specific in vivo inhibitor of bacterial secretin PulD. *Proc. Natl. Acad. Sci. U S A* https://doi.org/10.1073/pnas.0702963104 (2007).
19. Cinier, M. et al. Bisphosphonate adaptors for specific protein binding on zirconium phosphonate-based microarrays. *Bioconjug. Chem.* **20**, 2270–2277 (2009).
20. Correa, A. et al. Potent and specific inhibition of glycosidases by small artificial binding proteins (Affitins). *PLoS One* **9**, e97438 (2014).
21. Huet, S., Gorre, H., Perrocheau, A., Picot, J. & Cinier, M. Use of the nanofitin alternative scaffold as a GFP-ready fusion tag. *PLoS One* **10**, e0142304 (2015).
22. Mouratou, B., Béhar, G. & Pecorari, F. Artificial affinity proteins as ligands of immunoglobulins. *Biomolecules* **5**, 60–75. https://doi.org/10.3390/biom5010060 (2015).
23. Satsangi, J. et al. How to apply for and secure EU funding for collaborative IBD research projects. *J. Crohns Colitis* **10**, 363–370 (2016).
24. Goux, M. et al. Nanofitin as a new molecular-imaging agent for the diagnosis of epidermal growth factor receptor over-expressing tumors. *Bioconjug. Chem.* **28**, 2361–2371 (2017).
25. Garlich, J. et al. Discovery of APL-1030, a novel, high-affinity nanofitin inhibitor of C3-mediated complement activation. *Biomolecules* **12**, 432 (2022).
26. Hernot, S. *et al.* review latest developments in molecular tracers for fluorescence image-guided cancer surgery. www.thelancet.com/oncology **20** (2019).
27. Nini, A. et al. Evaluation of HER2 expression in urothelial carcinoma cells as a biomarker for circulating tumor cells. *Cytom. B. Clin. Cytom.* **98**, 355–367 (2020).
28. Half, E. et al. HER-2 receptor expression, localization, and activation in colorectal cancer cell lines and human tumors. *Int. J. Cancer.* **108**, 540–548 (2004).
29. Kim, H. J. et al. PET imaging of HER2 expression with an 18 F-fluoride labeled aptamer. *PLoS One* **14**, e0211047 (2019).
30. Warram, J. M. et al. Antibody-based imaging strategies for cancer. *Cancer. Metastasis Rev.* **33**, 809–822. https://doi.org/10.1007/s10555-014-9505-5 (2014).
31. Chames, P., Van Regenmortel, M., Weiss, E. & Baty, D. Therapeutic antibodies: Successes, limitations and hopes for the future. *Br. J. Pharmacol.* **157**, 220–233. https://doi.org/10.1111/j.1476-5381.2009.00190.x (2009).
32. Bai, J. W., Qiu, S. Q. & Zhang, G. J. Molecular and functional imaging in cancer-targeted therapy: Current applications and future directions. *Signal Transduct. Target Ther.* https://doi.org/10.1038/s41392-023-01366-y (2023).
33. Tolmachev, V., Orlova, A. & Sörensen, J. The emerging role of radionuclide molecular imaging of HER2 expression in breast cancer. *Sem. Cancer Biol.* **72**, 185–197. https://doi.org/10.1016/j.semcancer.2020.10.005 (2021).
34. Massicano, A. V. F., Marquez-Nostra, B. V. & Lapi, S. E. Targeting HER2 in nuclear medicine for imaging and therapy. *Mol. Imag.* https://doi.org/10.1177/1536012117745386 (2018).
35. Li, L. et al. SPECT/CT imaging of the novel HER2-targeted peptide probe 99mTc-HYNIC-H6F in breast cancer mouse models. *J. Nucl. Med.* **58**, 821–826 (2017).
36. Bragina, O. et al. Phase I Trial of 99mTc-(HE)3–G3, a DARPin-based probe for imaging of HER2 Expression in breast cancer. *J. Nucl. Med.* **63**, 528–535 (2022).
37. Wu, Y. et al. Imaging and monitoring HER2 expression in breast cancer during trastuzumab therapy with a peptide probe 99mTc-HYNIC-H10F. *Eur. J. Nucl. Med. Mol. Imag.* **47**, 2613–2623 (2020).
38. Sörensen, J. et al. First-in-human molecular imaging of HER2 expression in breast cancer metastases using the 111In-ABY-025 affibody molecule. *J. Nucl. Med.* **55**, 730–735 (2014).
39. Sörensen, J. et al. Measuring HER2-receptor expression in metastatic breast cancer using [68Ga]ABY-025 Affibody PET/CT. *Theranostics* **6**, 262–271 (2016).
40. Sarkaria, I. S. et al. Pafolacianine for intraoperative molecular imaging of cancer in the lung: The elucidate trial. *J Thorac. Cardiovasc. Surg.* **166**, e468–e478 (2023).
41. Gangadharan, S. et al. Multiinstitutional phase 2 clinical trial of intraoperative molecular imaging of lung cancer. *Ann. Thorac. Surg.* **112**, 1150–1159 (2021).
42. Marcion, G. et al. Nanofitins targeting heat shock protein 110: An innovative immunotherapeutic modality in cancer. *Int. J. Cancer* **148**, 3019–3031 (2021).
43. Feng, Y. et al. Quantitative pharmacokinetic and biodistribution studies for fluorescent imaging agents. *Biomed. Opt. Expr.* **15**, 1861 (2024).
44. Iaboni, M. et al. Fluorescence-based absolute quantification of near-infrared probes in tissue extracts for biodistribution analyses. *Anal. Biochem.* **677**, 115251 (2023).
45. Huet, S. et al. Targeted nanofitin-drug conjugates achieve efficient tumor delivery and therapeutic effect in an EGFRpos mouse xenograft model. *Mol. Cancer Ther.* **22**, 1343–1351 (2023).
46. Mouratou, B., Béhar, G., Paillard-Laurance, L., Colinet, S. & Pecorari, F. Ribosome display for the selection of sac7d scaffolds. *Method. Mol. Biol.* **805**, 315–331 (2012).
47. Gros, S. J. et al. Complementary use of fluorescence and magnetic resonance imaging of metastatic esophageal cancer in a novel orthotopic mouse model. *Int. J. Cancer* **126**, 2671–2681 (2010).
48. Leto, S. M. et al. Sustained inhibition of HER3 and EGFR is necessary to induce regression of HER2-amplified gastrointestinal carcinomas. *Clin. Cancer Res.* **21**, 5519–5531 (2015).

Acknowledgements

The authors would like to thank Gabriella Monaco, MD for her remarkable support during animal studies and Claudia Cabella, PhD for her invaluable guidance and support throughout this project.

Author contributions

M.I., F.C., F.A., F.L.C., F.B., A.M., L.P. and E.R. designed research; M.I., F.C., F.A., F.L.C., A.C., F.S., D.F., E.R.Z. and E.R. performed research; S.H., L.C., J.P. and F.C. contributed new product/ analytic tools; M.I., F.C., F.A., F.L.C., A.C., F.S., D.F., E.R.Z. and A.B. analyzed data; and M.I., F.C., F.A., F.L.C., S.H., L.C., J.P., L.P. and E.R. wrote the paper. All authors reviewed the manuscript.

Funding

Regione Piemonte,Project Fluomed POR FESR 2014/2020- Line A,Project Fluomed POR FESR 2014/2020- Line A,Project Fluomed POR FESR 2014/2020- Line A,Project Fluomed POR FESR 2014/2020- Line A,Project Fluomed POR FESR 2014/2020- Line A,Project Fluomed POR FESR 2014/2020- Line A.

Declarations

Competing interests

Bracco Imaging SpA, which is the affiliation of most of authors, is the applicant of a pending patent application, among else, the Nanofitin NF-Cys described in this manuscript. All other authors do not hold any competing interest.

Additional information

Supplementary Information The online version contains supplementary material available at https://doi.org/10.1038/s41598-025-93696-w.

Correspondence and requests for materials should be addressed to M.I.

Reprints and permissions information is available at www.nature.com/reprints.

Publisher's note Springer Nature remains neutral with regard to jurisdictional claims in published maps and institutional affiliations.